Supporting Information

Highly active and selective Li/MgO catalyst for methane transformation to C$_2$ hydrocarbons: Experimental and DFT study

Rohan Singh Pal,[a,b] Swati Rana,[a] Souvik Sadhu,[a] Tuhin Suvra Khan,[a,b] Mukesh Kumar Poddar,[a] Rajib Kumar Singha,[a] Suman Sarkar,[c] Rahul Sharma,[d] and Rajaram Bal,*[a,b]

[a]Light Stock Processing Division, CSIR-Indian Institute of Petroleum, Dehradun 248005, India. Fax: +91 135 2660202; Tel: +91 135 2525917.
[b]Academy of Scientific and Innovative Research (AcSIR), Ghaziabad- 201002, India
[c]Indian Institute of Technology, Jammu, NH-44, PO Nagrota, Jagti, Jammu and Kashmir-181221
[d]GAIL (India) Ltd, GAIL Training Institute
Plot No. 24,Sector 16-A,Noida,Uttar Pradesh
*Corresponding author E-mail: raja@iip.res.in

Catalyst characterization (General procedures)

The bulk phase composition of the fresh and spent catalysts was examined by XRD, using a Bruker D8 advanced X-ray diffractometer fitted with a Lynex eye high-speed strip detector and a Cu–K radiation source. Scans were collected over a range from 10° to 90° with a step of 0.05° s^{-1}. The specific surface areas and porosity of the calcined and spent samples were measured by nitrogen adsorption-desorption at 77 K on the Micromeritics ASAP 2020 Surface Area and Porosity Analyzer. The chemical compositions of the prepared catalysts were confirmed using an Inductively Coupled Plasma–Atomic Emission Spectroscopic (ICP–AES) study carried out with a Spectrometer model: PS 3000 UV (DRE) Leeman Labs, Inc. (USA). The Raman spectra of the catalysts were measured using a laser with a wavelength of 633 nm on a HORIBA Scientific LabRAM HR Evolution Raman spectrometer with an argon laser excitation source.

The range of scanned Raman shifts is 50 to 3000 cm^{-1}. The STEM images and EELS (Electron Energy Loss Spectroscopy) of the fresh catalyst were obtained using a NEORAM JEM-ARM200F Model. The HRTEM is aberration corrected. The Gun is stable COLD FEG. The HRTEM is equipped with STEM-HAADF attachment along with EELS analysis facility. The HRTEM was operated on 200kV acceleration voltage. X-ray photoelectron spectra (XPS) were recorded on a Thermo Scientific K-alpha X-ray photoelectron spectrometer. The CO_2-TPD reaction was performed with a Micromeritics, Auto Chem II 2920 (Micromeritics, GA, USA) instrument connected to a thermal conductivity detector to check the basicity of the prepared catalysts (TCD). In order to do this, a 50 mg catalyst was used for the test in a 30 ml min^{-1} He flow. To prevent any possible impurities, the sample was heated to 400°C and held for 30 minutes prior to the test. The sample was then cooled to 50°C, and then the sample was subjected to a 30 ml min^{-1} CO_2 flow for 1 hour to completely saturate the surface, followed by a 30 ml min^{-1} ultra-high purity He flow for 30 minutes to remove any physically adsorbed CO_2. After all of these pre-treatments, the catalyst was heated at a rate of 10 °C min^{-1} from 50 to 800°C to collect CO_2 desorption data.

To determine the oxidation state of the prepared catalyst, an XPS analysis was performed. X-ray photoelectron spectra (XPS) were recorded on a Thermo Scientific K-Alpha X-Ray photoelectron spectrometer, and binding energies (0.1 eV) were determined with respect to the position of the C 1s peak at 284.8 eV. The *in situ* IR studies were carried out in Nicolet iS50FT-IR (Thermo Scientific) spectrometer, equipped with a high temperature chamber fitted with ZnSe window with MCT detector and DRIFT mode. Prior to *in situ* DRIFT analysis, the samples were pretreated at 450 °C at a heating rate of 5 °C min^{-1} in N_2 flow (25 mL min^{-1}, , 2h activation time). Later the background spectra was taken for each sample at 450 °C. The required gases (CH$_4$, O$_2$, N$_2$) were introduced into the chamber, and the spectra were taken at 450 °C itself for 5 h, till the first hour the spectra was taken right after the introduction of the

required gases denoted as 1 min, then 2 min, 5min, 10 min, 30 min and 60 min and then spectra taken at every 1 h interval.

In-Situ Raman experiments were done in HORIBA Scientific instrument equipped with OLYMPUS confocal microscope, Labram detector made by CCD (charged coupled device) and LINKAM-CCR1500 in-situ high temperature reaction cell. Before each test, the sample was pre-treated in pure N_2 at a flow rate of 15 ml min^{-1} for 2 hours, after which a flow of feed gas (CH_4+O_2 in 1:2 , Flow =15 ml min^{-1}) was fed and after stabilisation for 30 minutes at each temperature, spectra were acquired using a 633 nm laser (He/Ne power source).

Electron paramagnetic resonance (EPR) spectra were collected at ambient temperature (at room temperature) on a Bruker Biospin, Germany EMX micro A200-9.5/12/S/W to investigate the formation of superoxide species/oxygen vacancy on the catalyst surface. The sample was placed in the capillary tube, and the experimental parameters of EPR were as follows: microwave frequency (9.400 GHz), microwave power (0.715 mW), modulation frequency (100 kHz), modulation amplitude (3.00 G), and sweep time (76.8 s).

Activity Measurements

The catalytic activity of the Li/MgO catalyst was tested at ambient pressure in a fixed-bed down-flow reactor. A quartz tube reactor with an inner diameter of 6 mm is used for the reaction. Typically, 0.30gm of catalyst is loaded in between two quartz wool plugs in the centre of a quartz tube reactor and then heated to the target temperature. Three mass flow controls were used to monitor the flow rates of the reactants CH_4, O_2, and N_2 steam. All experiments are conducted with a CH_4:O_2:N_2 volume ratio of 2:1:7. The total flow rate of the feed gas is 18.75 mL min^{-1}, 37.5 mL min^{-1}, 56.25 mL min^{-1}, and 75 mL min^{-1}, which results in a gas hourly space velocity of 3750 mL h^{-1} g^{-1}, 7500 mL h^{-1} g^{-1}, 11250 mL h^{-1} g^{-1}, and 15000 mL h^{-1} g^{-1}, respectively. Before measuring catalytic activity, each catalyst is activated for 2 hours at 450

°C with pure oxygen (flow: 15 ml/min), then switched to N_2 flow until the reaction temperature is attained, and then switched to feed gas in a 7:2:1 ratio of N_2: CH_4: O_2. The methane coupling products were analyzed by using an Agilent 8890 (G3540A) GC system fitted with a HayeSep Q and Molsieve 13X column and a TCD detector for the analysis of N_2, O_2, CO, CO_2, and a GS-GASPRO column and a FID detector for the analysis of CH_4, C_2H_6, C_2H_4, C_3H_8, C_3H_6 etc. The carbon and mass balances were estimated to be within +2%. The methane conversion (XCH_4), C_2 selectivity (S_{C2}), and C_2 yield (Y_{C2}) in this study were calculated by using the following equations:

$$\text{Methane Conversion (\%) } X_{CH4} = \frac{moles\ of\ CH4\ consumed}{moles\ of\ CH4\ in\ Feed} \times 100$$

$$\text{C}_2 \text{ Selectivity (\%) } S_{C2} = \frac{2\ \times\ moles\ of\ C2\ Hydrocarbon}{moles\ of\ CH4\ consumed} \times 100$$

$$\text{C}_2 \text{ Yield (\%) } Y_{C2} = \frac{CH4\ Conversion\ \times\ C2\ Selectivity}{100}$$

Computational Method

All electron spin-polarized density functional theory (DFT), as implemented in DMol[3] package of Material Studio 8 (Biovia, San Diego, USA) having double numerical plus polarization (DNP) basis set.[1] The MgO crystal was cleaved along the (100) direction to build the MgO(100) surface. The MgO(100) surface slab was made of four layers and 20 Å vacuum was added along the z-direction. Generalized gradient approximation (GGA) Perdew Burke Ernzerhof (PBE) exchange correlation functional[2] was used along with effective core potentials to describe the electron-core interaction. The reaction energies and activation barriers were obtained using the geometry optimization and transition state calculations as implemented in

Materials Studio DMol[3]. During the geometry optimization the two bottom layers of MgO(100) surface slab were kept fined to their bulk position, whereas the top two along with the adsorbates were allowed to relax. For the transition state (TS) calculations linear synchronous transit/quadratic synchronous transit (LST/QST) method was used.[3] For both the geometry optimizations and transition state calculations convergence criteria were kept at 0.0005 eV, 0.1 eV/Å, and 0.005 Å with respect to energy, force, and atom displacement, respectively. The k-points sampling of 2x2x1 were used for all the calculations along with thermal smearing of 0.01 Ha.

Synthesis procedure of 2%Mn/5%Na$_2$WO$_4$/SiO$_2$ catalyst

2%Mn/5%Na$_2$WO$_4$/SiO$_2$ catalyst for comparison purpose is synthesized by sequential wet impregnation method by using Mn(NO$_3$)$_2$.xH$_2$O and Na$_2$WO$_4$.2H$_2$O precursors ,and calcined at 800 °C. The detailed catalytic activity of this catalyst is shown below in figure S6
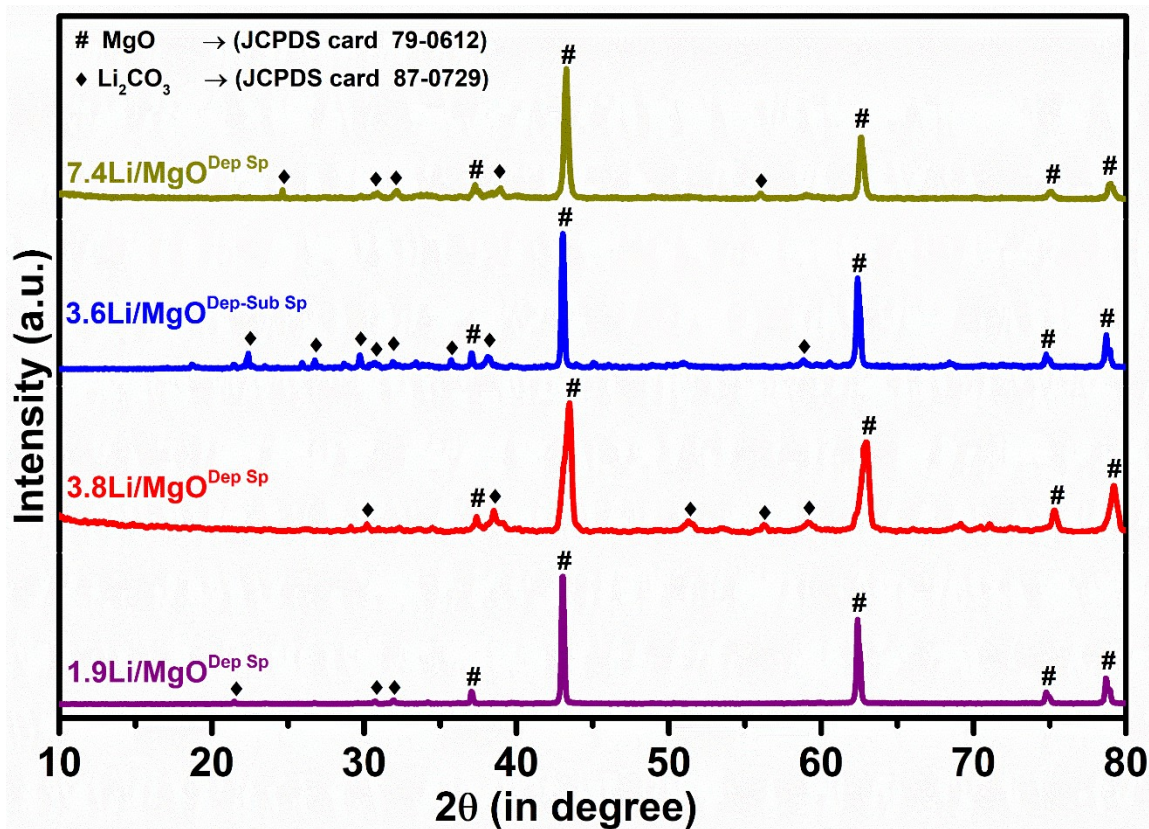

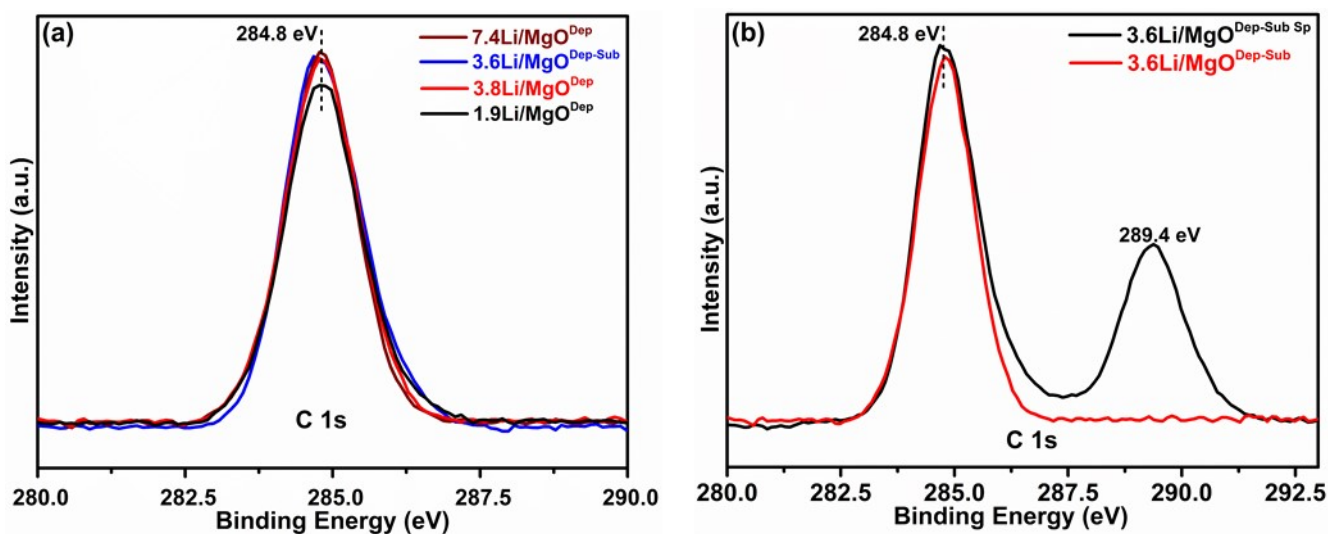**Figure S1** Spent XRD pattern of different wt.% Li/MgO spent catalyst

Figure S2 (a) C1s XPS spectra for all prepared catalyst (b) comparison of C1s XPS spectra of 3.6Li/MgO[Dep-Sub] Fresh and spent catalyst ;Sp indicates Spent catalyst
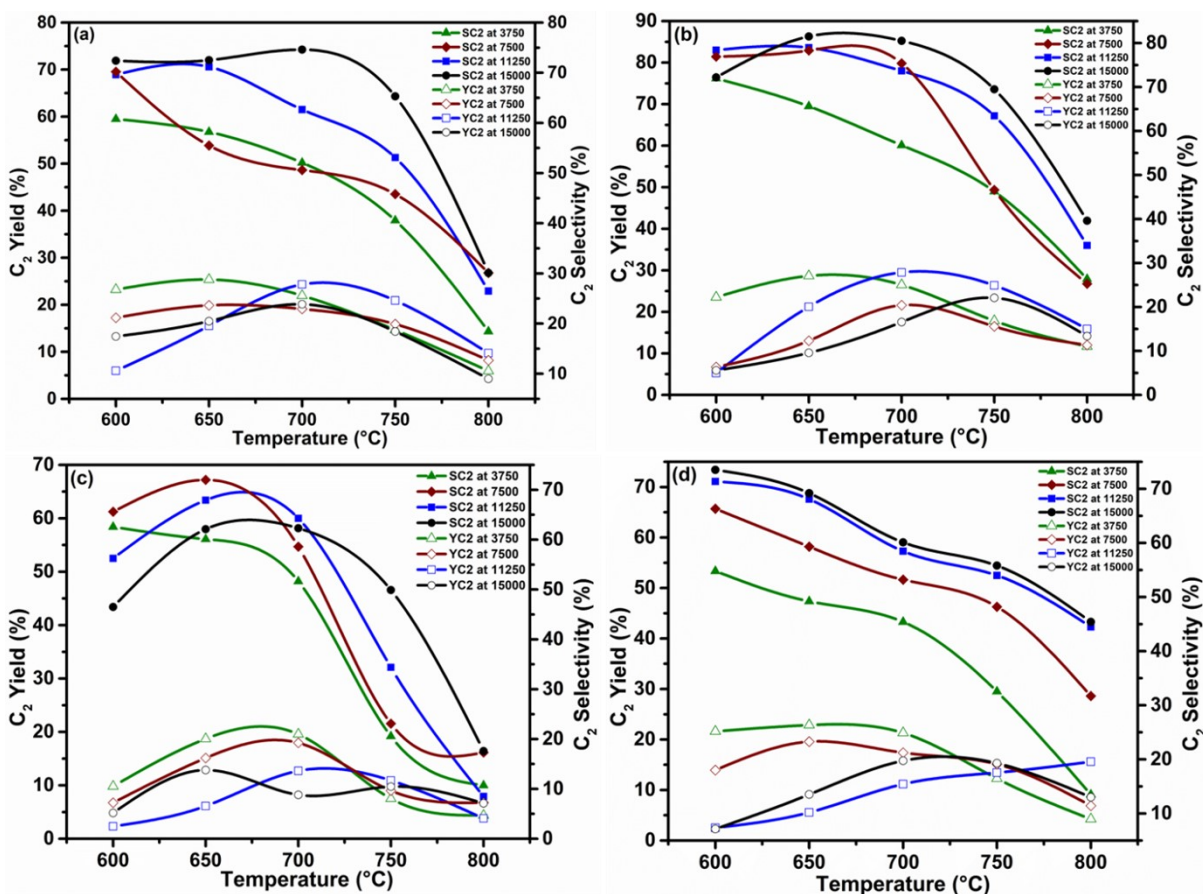

Figure S3 Effect of GHSV (in mL h^{-1} g[cat.][-1]) on total C_2 Selectivity and total C_2 Yield as a function of temperature for (a)1.9Li/MgO[Dep] (b)3.6Li/MgO[Dep-Sub] (c)3.8Li/MgO[Dep] (d)7.4Li/MgO[Dep]

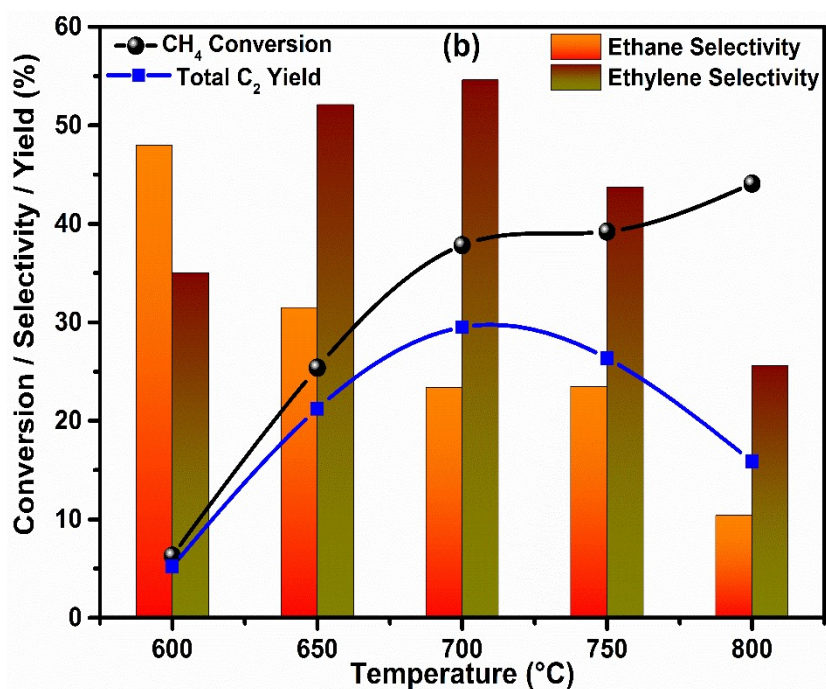(SC_2=Selectivity of C_2 hydrocarbons, YC2= Yield of C_2 hydrocarbons)

Figure S4 Represents the CH_4 Conversion, C_2 Yield, and Ethane and Ethylene Selectivity as a Function of Temperature for a 3.6Li/MgO[Dep-Sub] catalyst.
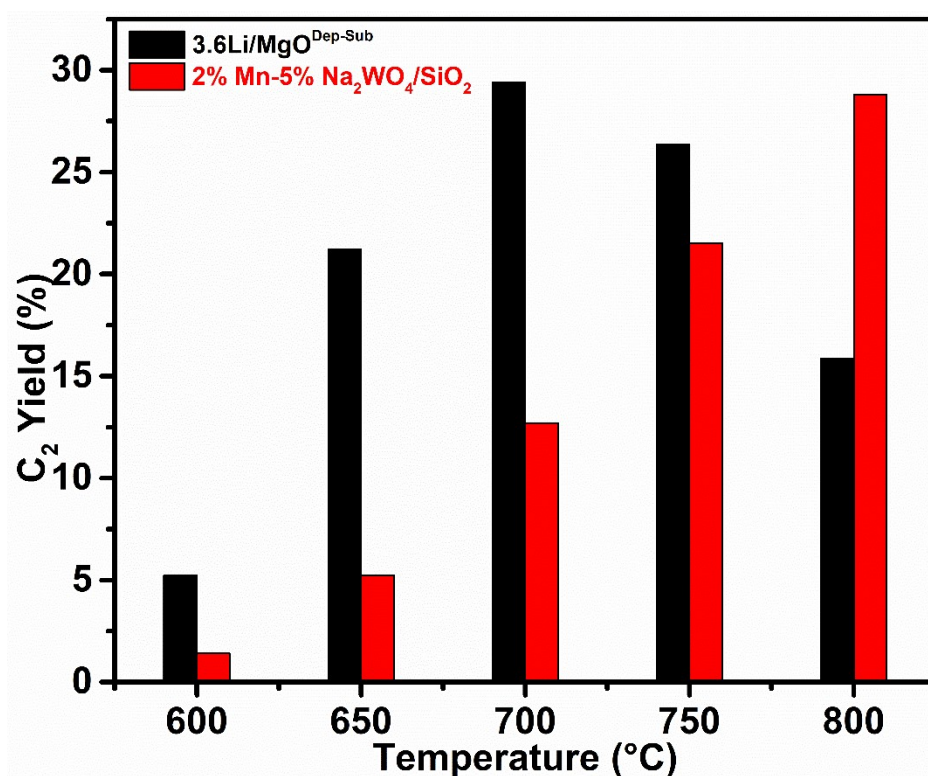

Figure S5 represents the comparison of C_2 yield between 3.6Li/MgO[Dep-Sub] catalyst and 2%Mn/5%Na_2WO_4/SiO_2 catalyst
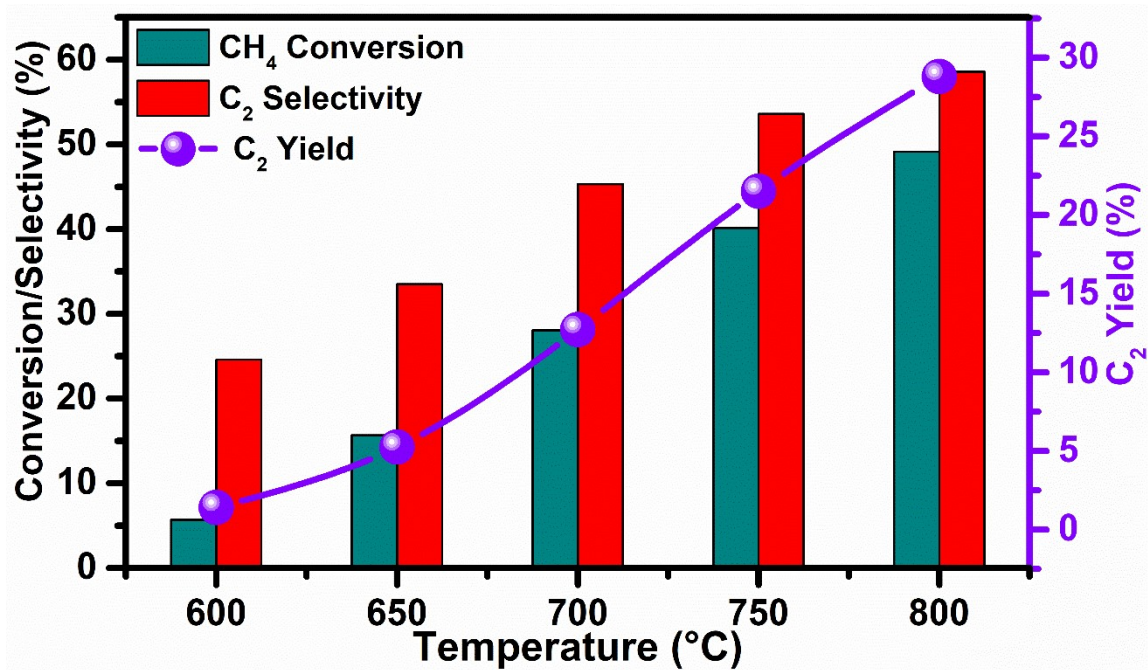
Figure S6 catalytic activity of 2%Mn/5%Na$_2$WO$_4$/SiO$_2$ catalyst Operating conditions: T = 600-800 °C, GHSV = 11250 ml·g^{-1}·h^{-1}, 0.3 g catalyst, CH$_4$:O$_2$:N$_2$=2:1:7, P = 1 atm
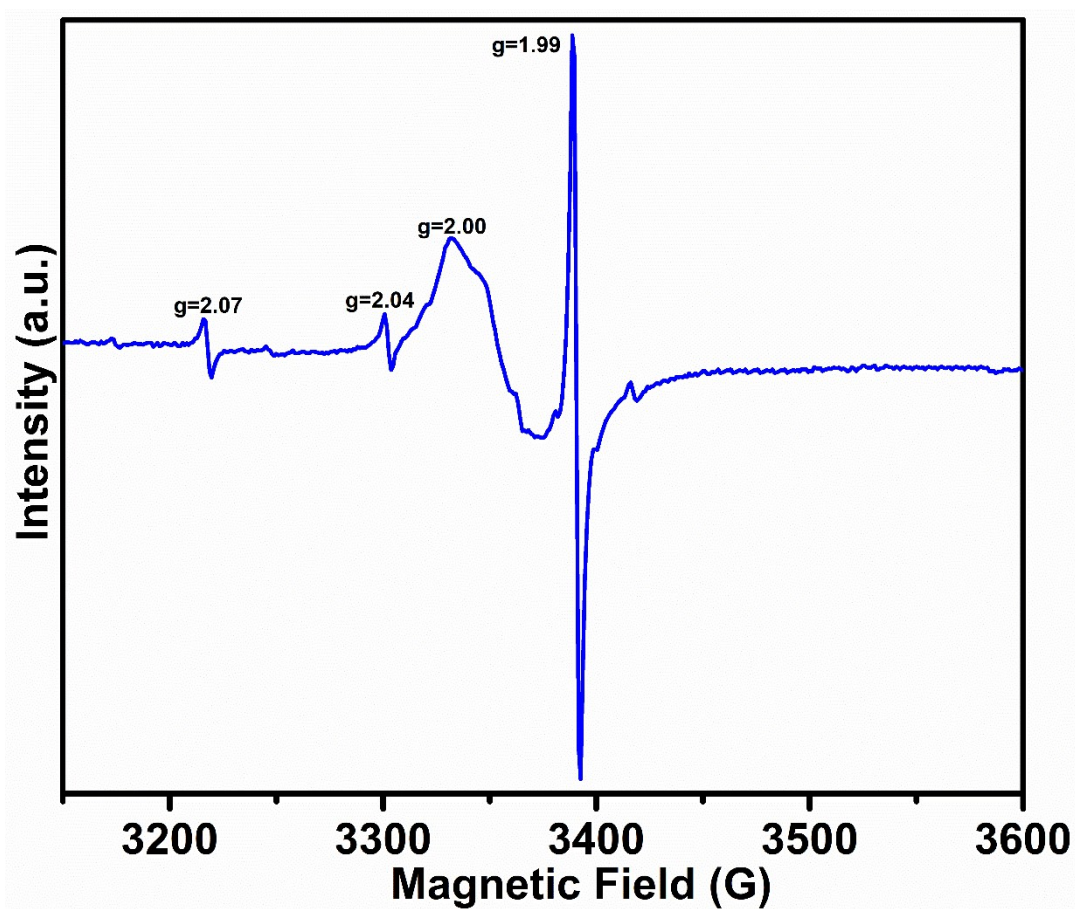

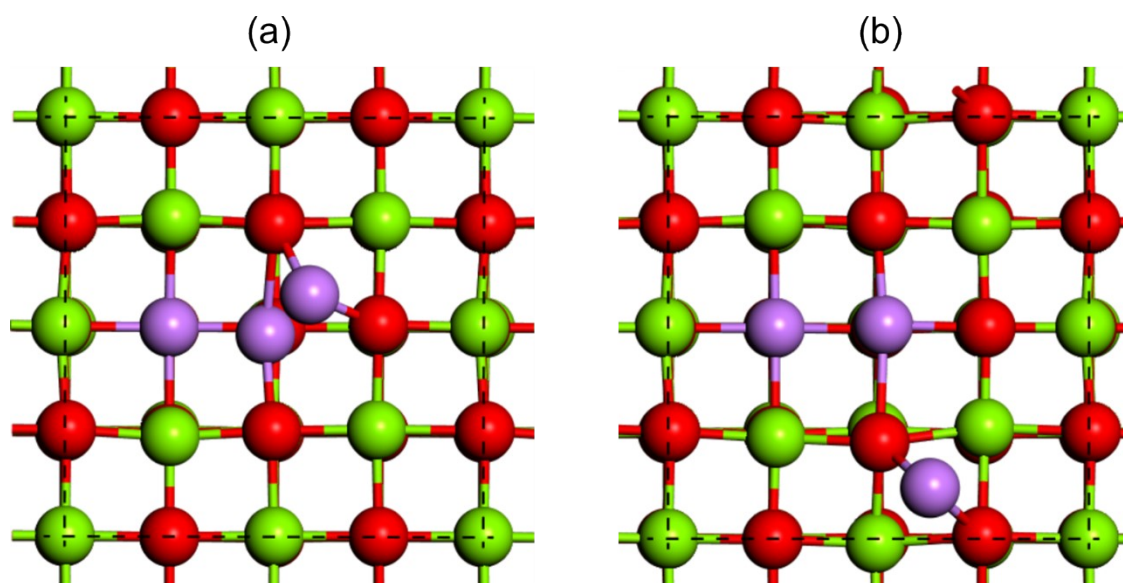**Figure S7** representing EPR spectra of 3.6Li/MgO$^{Dep-Sub}$ catalyst at Room temperature

Figure S8. DFT optimized geometry of Li$_3$-MgO(100) configuration (a) Li added near the oxygen vacancy site, (b) Li added away from oxygen vacancy site. Color code: Mg (green), O (red), Li (purple).
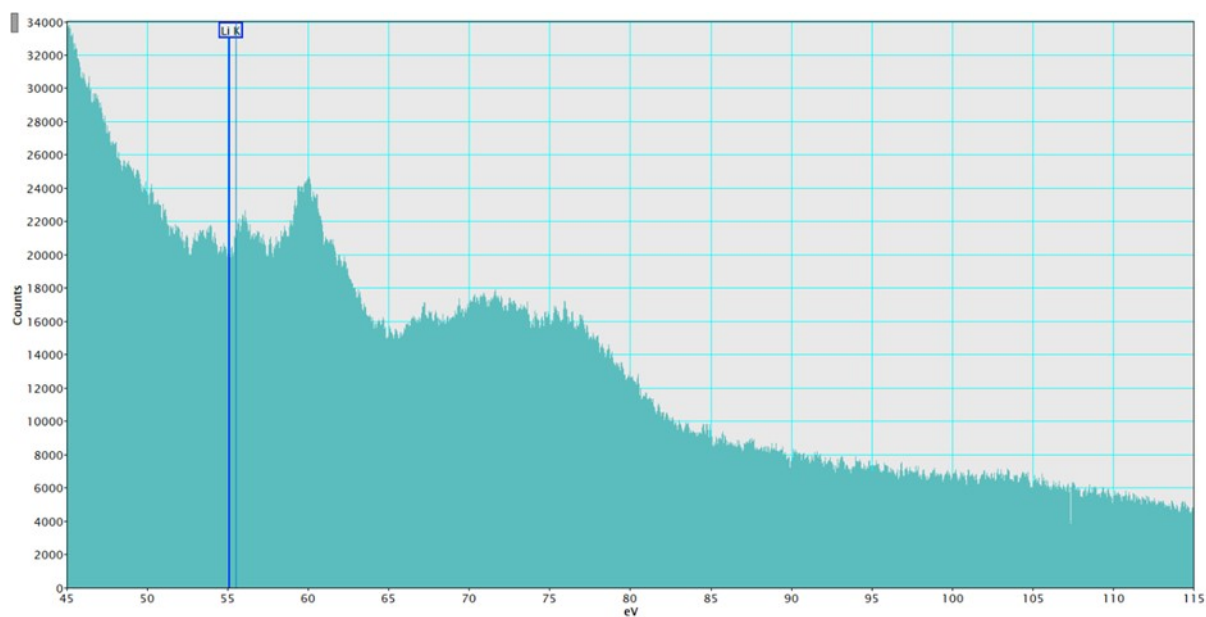

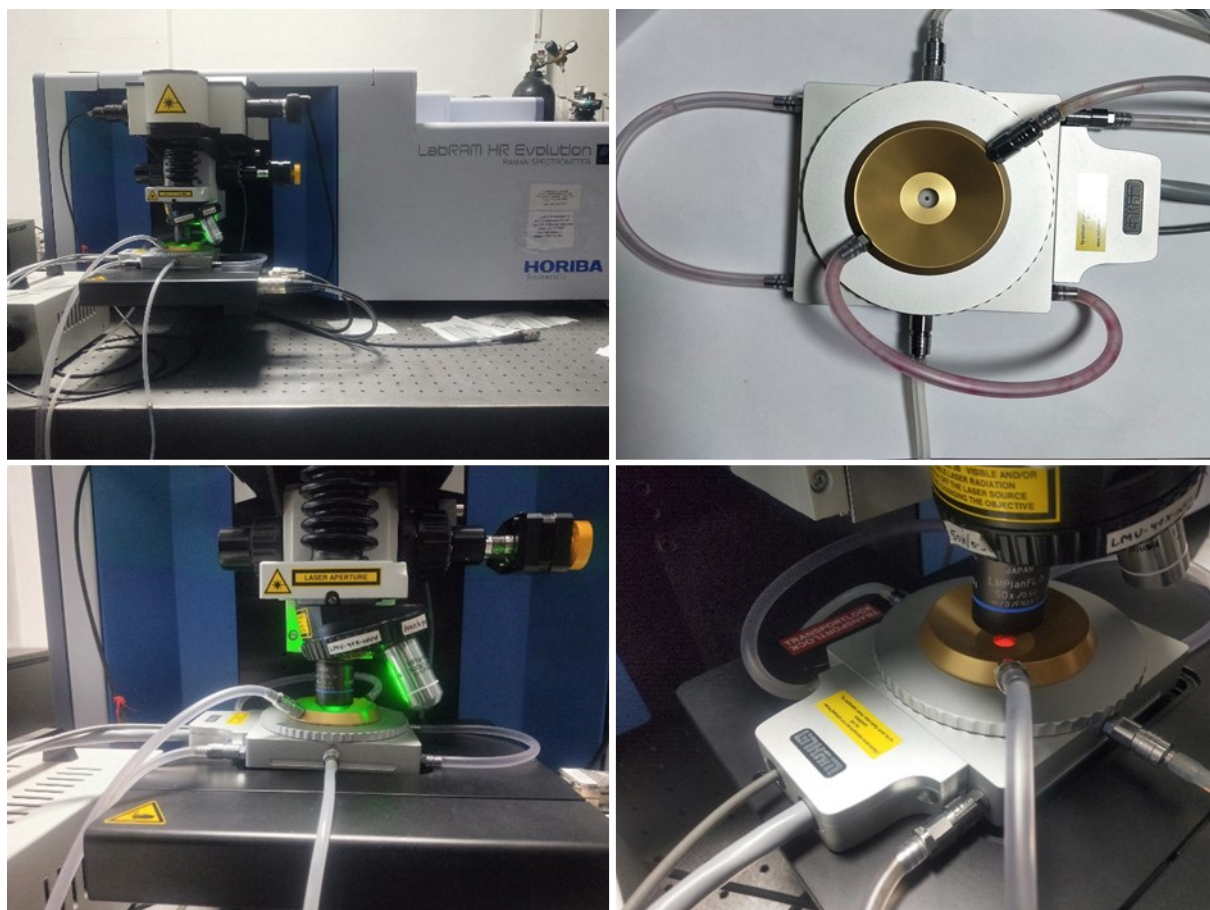**Figure S9.** EELS spectra of 3.6Li/MgO$^{Dep-Sub}$ catalyst

In-situ Raman Spectroscopic Instrument Setup

Table S1 average crystallite size D of MgO (in nm) from XRD

Catalyst	Average crystallite size D (nm) MgO
MgO	22.56
1.9Li/MgO^{Dep}	33.84
3.6Li/MgO$^{Dep-Sub}$	30.39
3.8Li/MgO^{Dep}	35.89
7.4Li/MgO^{Dep}	40.42

Table S2 Comparison of the catalytic activity of our catalyst with some of the catalysts reported in literature.

S.No.	Catalyst	Temp. (°C)	CH$_4$ Conversion (%)	C$_2$ Selectivity (%)	C$_2$ Yield (%)	Ref.
1	Li-MgO	780	25.4	41.2	-	4
2	Sr–Li/MgO	750	22.8	50-55	-	5
3	Li-MgO	750	15.6	29	5	6
4	Li/MgO/Al$_2$O$_3$/FeCrAl	850	38.3	27.1	8	7
5	11.2% Li/MgO	750	9.2	69.3	-	8
6	22.4% Li/MgO	750	5.1	74.3	-	8
7	Ce/Na/CaO	750	9.7	80.8		9
8	SrO/La$_2$O$_3$/SA-5205	800	30.9	-	19.9	10
9	Alkali Chloride-Mn-Na$_2$WO$_4$/SiO$_2$	750	55	33.6	26	11
10	Mn-Na$_2$WO$_4$/SiO$_2$	800	32.7	58.6	19.2	12
11	3%Ce/5% Na$_2$WO$_4$/TiO$_2$	800	49	56.4	27.6	13
12	TiO$_2$-doped Mn$_2$O$_3$-Na$_2$WO$_4$/SiO$_2$	720	26	76	-	14
13	Mn–Na$_2$WO$_4$/SiO$_2$	800-875	20-30	70-80	-	15
14	La$_2$Ce$_{1.5}$Ca$_{0.5}$O$_7$	750	32	76	22.5	16
15	**3.6Li/MgO$^{\text{Dep-Sub}}$**	**700**	**37.8**	**78**	**29.4**	**This Work**

References

1 B. Delley, *The Journal of Chemical Physics*, 1990, **92**, 508–517.

2 J. P. Perdew, K. Burke and M. Ernzerhof, *Physical Review Letters*, 1997, **78**, 1396–1396.

3 T. A. Halgren and W. N. Lipscomb, *Chemical Physics Letters*, 1977, **49**, 225–232.

4 Z. Gao, J. Zhang and R. Wang, *Journal of Natural Gas Chemistry*, 2008, **17**, 238–241.

5 V. I. Alexiadis, J. W. Thybaut, P. N. Kechagiopoulos, M. Chaar, A. C. Van Veen, M. Muhler and G. B. Marin, *Applied Catalysis B: Environmental*, 2014, **150-151**, 496–505.

6 S. Arndt, U. Simon, S. Heitz, A. Berthold, B. Beck, O. Görke, J.-D. . Epping, T. Otremba, Y. Aksu, E. Irran, G. Laugel, M. Driess, H. Schubert and R. Schomäcker, *Topics in Catalysis*, 2011, **54**, 1266–1285.

7 Z. Zhang and S. F. Ji, *Advanced Materials Research*, 2014, **1004-1005**, 648–652.

8 K. Qian, R. You, Y. Guan, W. Wen, Y. Tian, Y. Pan and W. Huang, *ACS Catalysis*, 2020, **10**, 15142–15148.

9 J. G. A. Pacheco Filho, J. G. Eon and M. Schmal, *Catalysis Letters*, 2000, **68**, 197–202.

10 V. R. Choudhary, S. A. R. Mulla and B. S. Uphade, *Fuel*, 1999, **78**, 427–437.

11 N. Hiyoshi and T. Ikeda, *Fuel Processing Technology*, 2015, **133**, 29–34.

12 H. R. Godini, A. Gili, O. Görke, S. Arndt, U. Simon, A. Thomas, R. Schomäcker and G. Wozny, *Catalysis Today*, 2014, **236**, 12–22.

13 V. Jodaian and M. Mirzaei, *Inorganic Chemistry Communications*, 2019, **100**, 97–100.

14 P. Wang, G. Zhao, Y. Wang and Y. Lu, *Science Advances*, DOI:10.1126/sciadv.1603180.

15 S. Arndt, T. Otremba, U. Simon, M. Yildiz, H. Schubert and R. Schomäcker, *Applied Catalysis A: General*, 2012, **425-426**, 53–61.

16 J. Xu, Y. Zhang, Y. Liu, X. Fang, X. Xu, W. Liu, R. Zheng and X. Wang, *European Journal of Inorganic Chemistry*, 2018, **2019**, 183–194.

.